



Sensing nitrite by iron-nitrogen-carbon oxygen reduction electrocatalyst

Valerio C.A. Ficca^a, Carlo Santoro^{b,*}, Enrico Marsili^{c,*}, Williane da Silva Freitas^a, Alexey Serov^d, Plamen Atanassov^e, Barbara Mecheri^{a,*}

^a Department of Chemical Science and Technologies, University of Rome Tor Vergata, Via della Ricerca Scientifica, Rome 00133, Italy

^b Department of Material Science, University of Milan Bicocca, U5 Via Cozzi 55, Milan 20125 Italy

^c Department of Chemical and Materials Engineering, Nazarbayev University, 53 Kabanbay Batyr Avenue, Nur-Sultan 010000, Kazakhstan

^d Oak Ridge National Laboratory, Electrification and Energy Infrastructures Division, Oak Ridge, TN 37831, USA

^e Chemical and Biomolecular Engineering, National Fuel Cell Research Center, University of California, Irvine, CA 92697 USA



ARTICLE INFO

Article history:

Received 12 October 2021

Accepted 28 October 2021

Available online 1 November 2021

Keywords:

Platinum group metal-free

Oxygen reduction reaction

Rotating disk electrode

Biosensor

Nitrite detection

ABSTRACT

Nitrite contamination of groundwater is a concerning consequence of anthropic activity. The electrochemical detection of nitrite in water is based on direct electrocatalytic oxidation of nitrite over modified electrodes. However, drawbacks associated to the high oxidation potential required, oxide layer formation, and O₂ interference are present. Considering the recent availability and low cost of platinum-group-metal-free (PGM-free) electrocatalyst, a new sensing strategy is presented based on this class of material commonly used for oxygen reduction reaction (ORR) in fuel cells. The working principle relies on the inhibition of ORR active sites of PGM-free caused by the interaction with nitrite. The parameters of interest for the ORR inhibition were determined through cyclic voltammetry and chronopotentiometry using a rotating disk electrode to minimize oxygen diffusion limitations at the working electrode. The linearity range of the sensor was 1–100 μM, with a sensitivity of 3.4 mV μM⁻¹, and a limit of detection (LOD) in the sub-μM range. Based on the optimization of the electrocatalyst thickness and its reusability, the cost of 1 USD for ~2000 tests was calculated.

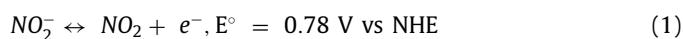
© 2021 Elsevier Ltd. All rights reserved.

1. Introduction

Nitrite and nitrate are inorganic compounds used in both food industry and agriculture as food preserving additive and fertilizers, respectively. The release of nitrite and nitrate in freshwater and aquifers is mainly caused by the washed out of fertilizers, leakage from septic tanks, erosion of natural deposits, natural nitrification due to the presence of ammonia, and incomplete denitrification in wastewater treatment plants. Nitrogen species in water bodies contribute to the algal blooms and the subsequent eutrophication phenomena. Consequently, their discharge limit is stringent, which requires a rapid and accurate detection. Among nitrogen compounds, nitrite has the most stringent limit: US EPA established 1 mg L⁻¹ (as N) as maximum contaminant level (MCL) goal [1], while EU MCL standard for drinking-water is 0.5 mg L⁻¹ (Council Directive 98/83/EC) [2].

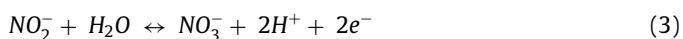
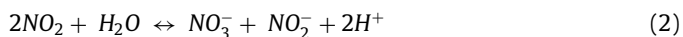
Numerous methods for the detection and determination of nitrite and/or nitrate have been previously reported, including spectrophotometry [3], chemiluminescence [4], electrochemistry [5,6], chromatography [7], spectrofluorimetry [8] and electrochemiluminescence [9,10]. Comprehensive reviews of these methods are reported in literature [11,12]. Commercial methods that combine chromatographic separation with spectroscopy have a limit of detection (LOD) of 3.6 μM (Aquamonitrix, Ireland) and reagent-based spectroscopy kits have a LOD as low as 0.015 μM (Hach, Germany). However, those methods generally require expensive equipment or material and might have long response time. Furthermore, sample pretreatment is often needed to decrease turbidity and continuous detection is not feasible, which limit their large-scale applications.

Electrochemical sensors for nitrite detection are based on the direct electrocatalytic oxidation of nitrite at the electrode surface, following a two-step mechanism on platinum, gold, and glassy carbon electrodes. The first step involves an electron transfer to form nitrogen dioxide (Eq. (1)) followed by its disproportionation in aqueous solution (Eq. (2)):



* Corresponding authors.

E-mail addresses: carlo.santoro@unimib.it (C. Santoro), enrico.marsili@nu.edu.kz (E. Marsili), barbara.mecheri@uniroma2.it (B. Mecheri).



Eq. (3) is the overall reaction [13–16]. Due to the high potential required, sensors based on nitrite oxidation have several drawbacks, namely oxide layer formation and instability of the sensing interface. In addition, this methodology is prone to interferences arising from O_2 dissolved into the electrolyte solution.

Nitrite sensors containing platinum group metal (PGM) such as Pt, Pd, Ag and Au have been reported, with a LOD in the range 0.1–0.5 μM [11,12]. However, the high cost of PGM is not feasible for large-scale monitoring. Nitrite shows high electroactivity on glassy carbon electrodes with the possibility of reducing the LOD and extending the linear range through electrode modification. In addition, modifications inhibit the electrode contamination, leading to analytical performance improvements, especially for wastewater and biological samples. Electrode modification using carbon nanotubes (CNT) and reduced graphene oxides (RGO) were recently reviewed [17,18]. While the performance of these two categories of sensors is similar, the RGO-based sensors have a lower LOD than CNT-based sensors (0.03–23.5 μM vs. 0.006–30 μM , respectively). Other sensing systems reported are based on carbon fiber paper [19] and graphene-coated filter paper [20]. Most of these carbon-based electrodes use the standard three electrodes setup for electrochemical tests, exploiting amperometry, potentiometry, cyclic voltammetry, differential pulse voltammetry, or square wave voltammetry as sensing methodologies [11,12,21,22].

All the above examples of electrochemical nitrite sensors are based on the specific oxidation of nitrite over a carbonaceous based material. In this work, a new methodology is explored, which uses the inhibition of the oxygen reduction reaction (ORR) electrocatalysis of the platinum-group-metal-free (PGM-free) catalysts family upon interaction with nitrite. This new methodology hence is not affected by the abovementioned issues related to nitrite oxidation, due to lower potential required for the ORR.

PGM-free materials are nanostructured carbon-based electrocatalysts developed for Pt replacement in acid or alkaline fuel cells and possess a peculiar heme-like active site denoted as $\text{Fe-N}_x\text{-C}$. These active sites are engineered to obtain an atomically dispersed metal (usually Fe) coordinated with up to 4 nitrogen atoms and embedded in a conductive carbon matrix [23–25].

PGM-free electrocatalyst catalyzes ORR and the mechanism followed to convert oxygen to water is summarized in Table S1 and involves four protons and four electrons per oxygen molecule, with a rate-determining step considered to be the first electron transfer. The reaction is pH-dependent and follows an Inner Helmholtz sphere mechanism from pH 0 up to pH 10.5, above which an Outer Helmholtz sphere mechanism takes place due to OH^- adsorbed species [26]. Compared to hydrogen oxidation, the ORR is a sluggish reaction, and a catalyst is required. The role of PGM-free electrocatalysts is the binding of oxygen molecules and their conversion through the specific $\text{Fe-N}_x\text{-C}$ active site [23–27]. Comprehensive studies on PGM-free materials obtained with different precursors have been already published [23–31].

Since the ORR on $\text{Fe-N}_x\text{-C}$ active sites is similar to that occurring in nature over M-N_4 macrocycles containing transition metals [29,32] or heme-like structures, other aspects can be compared. This is especially true in terms of contaminants able to bind Fe, like CN^- , H_2S , and NO_2^- , effectively impacting the ORR kinetic activity of the catalysis. Regarding the nitrite molecule, the poisoning is considered selective [33,34] and it is correlated to the presence of the atomic metal into the $\text{Fe-N}_x\text{-C}$ coordination, which forms a stable nitrosyl adduct bond. The effect of nitrite poisoning on the ORR activity of PGM-free has been previously reported [33–35] and

was utilized to quantify the number of catalytic active sites in the material [33,34]. As the active sites of the $\text{Fe-N}_x\text{-C}$ type are exposed to nitrite, specific chemisorption occurs with a consequent decrease of the ORR electrocatalytic activity [35]. As a result, the quantitative correlation of nitrite content to the electrochemical behavior reported is possible by monitoring either the trends of the faradaic peaks in cyclic voltammetry or the halfwave potentials decrease in linear sweep voltammetry, in the presence of different nitrite concentrations. At specific set potential, the current delivered by the system is negatively affected upon nitrite interaction.

In this work, the preliminary assessment for an electrochemical sensor for nitrite detection based on ORR inhibition of $\text{Fe-N}_x\text{-C}$ sites upon interaction with the nitrite molecule is proposed. The sensor is based on a glassy carbon rotating disk electrode (RDE) modified with a $\text{Fe-N}_x\text{-C}$ electrocatalyst layer, operated with a rotor in a three-electrode configuration. The working principle is based on the monitoring of the ORR potential variation at a specific set current density as a function of the increase in nitrite concentration. Sensor selectivity, as well as stability and reversibility, were also assessed.

2. Materials and methods

2.1. Electrocatalyst synthesis

The PGM-free electrocatalyst used in this work was synthesized using the Sacrificial Support Method (SSM) as previously reported [35–37]. Briefly, benzimidazole (BZIM) and iron nitrate, used as nitrogen, carbon and metal source, were mixed with low surface area monodispersed silica (OX50, 45 $\text{m}^2 \text{g}^{-1}$) used as template agent. The mixture was pyrolyzed in a controlled atmosphere (UHP nitrogen, 100 $\text{cm}^3 \text{min}^{-1}$) at 900 $^\circ\text{C}$ for 45 min. The resulting product underwent an acid washing procedure in 24 wt.% HF for 48 h to remove silica and undesired byproduct compounds like carbides, carbo-nitrides, metallic iron, and oxides. After the acid washing, the electrocatalyst was washed with distilled water until neutral pH was achieved. The resulting materials was dried overnight at 80 $^\circ\text{C}$. Lastly, a ball milling treatment of 20 min at 450 rpm was performed to homogenize the fine powder. The resulting fine-dispersed powder was labelled as Fe-BZIM.

2.2. Experimental strategy

Three different electrocatalyst loadings and two concentrations of binder (Nafion) were chosen accordingly to previous experiments [35]. This corresponds to six experimental conditions as summarized in Schematic S1. Each condition was tested in two replicates, prepared at different times. The concentrations were chosen according to the following criterium: 0.17 mg cm^{-2} was the former value used for the mM nitrite concentration range and hence can be considered as the upper limit of electrocatalyst loading. On the other side, considering the electrode employed for this study with a 5 mm diameter, catalyst loading below 0.1 mg cm^{-2} causes deposition problems, thus this value was set as the lower loading limit. An intermediate loading of 0.135 mg cm^{-2} was included between the high and low limits. Two different Nafion contents as binder were used: 150 $\mu\text{L mL}^{-1}$ and 100 $\mu\text{L mL}^{-1}$, the former being a standard Nafion content already employed for benchmark purpose. It was previously shown that both Nafion content and catalyst loading affected the electrocatalytic response in ORR in the mM range [35], hence the optimal conditions in terms of homogeneous electrocatalyst dispersion and Nafion content for the μM range must be investigated and optimized. Linearity ranges were checked at different values extrapolated from CVs and chronopotentiometry or chronoamperometry were run to investigate the sensing ability of the system.

Table 1

Ink composition, electrocatalyst loading normalized to electrode surface, and sample names. Nafion content referred to ink volume of 1 mL.

Nafion content ($\mu\text{L mL}^{-1}$)	Electrocatalyst loading (mg cm^{-2})	Sample name
150	0.100	0.1–150
150	0.135	0.135–150
150	0.170	0.17–150
100	0.100	0.1–100
100	0.135	0.135–100
100	0.170	0.17–100

2.3. Ink preparation and electrode modification

Two batches of ink were prepared as follows: the first batch (total volume 1 mL) was obtained by mixing 4 mg of Fe-BZIM, 850 μL ethanol (Ethanol absolute AnalaR Normapur, VWR Chemicals), 150 μL of diluted (with Millipore water, 18.2 M Ωcm @ 25 °C) Nafion 0.5 wt.% solution (5 wt% in lower aliphatic alcohols and water, Aldrich). The second batch (total volume 1 mL) differs from the first one for the Nafion content and have the following composition: 4 mg of Fe-BZIM, 900 μL ethanol, 100 μL of diluted Nafion 0.5 wt.% solution. The suspensions were ultrasonicated for 45 min at a temperature of 15–19 °C to perform the first electrocatalyst deposition on a glassy carbon electrode (Pine AFE3T050GC). The ultrasonic treatment was repeated for 30 min to perform the second deposition and 15 extra minutes for further depositions in the same day. The ink was drop-casted on the electrode surface using a micropipette to final loadings of 0.1, 0.135, and 0.17 mg cm^{-2} , as summarized in Table 1, and hence dried 1 min at 40 °C in a muffle oven.

2.4. Electrochemical set up and nitrite detection tests

A first set of cyclic voltammetry (CV) was run at increasing nitrite concentrations in a three-electrode glass cell filled with 0.1 M Phosphate Buffer Solution (PBS), as electrolyte solution, Saturated Calomel Electrode (SCE, AMEL 303/SCG/12) as reference electrode, graphite rod as counter electrode (6 mm diameter), and a Rotating Disk Electrode (RDE, 5 mm diameter) as working electrode (Pine AFE3T050GC). The cell was connected to a VMP3 Potentiostat (Bio-Logic) controlled by EC-Lab software (Bio-Logic). Before electrochemical tests, the catalytic layer was activated by acquiring CVs in a 1.05–0.05 V vs RHE potential window at 20, 50, 500 mV s^{-1} for 4, 6, 150 cycles, in N_2 -saturated PBS. After activation, CVs were acquired at 5 mV s^{-1} between 0.95 and 0.45 V vs RHE (data averaged over 3 scans) in O_2 -saturated electrolyte, containing increasing concentration of nitrite. After the addition of nitrite, the solution was stirred and subsequently purged with oxygen for 3 min. The procedure was repeated for all the concentration steps (1, 2, 5, 10, 20, 50, 100 μM) and the resulting CV curves were background-subtracted and iR-corrected.

After the preliminary CV tests, chronopotentiometry (CP) or chronoamperometry (CA) were performed by setting the current density values corresponding to at least the half-maximum of the CV faradaic peak, or the potential values lower than the faradaic peak potential plus 0.03 V, respectively. The averaged potential, or current density, variations after each nitrite addition were collected and the data extrapolated accordingly to the following protocol. The test started after 1000 s of stabilization, spinning the electrode at the rotation rate of 1600 rpm with the oxygen flow lifted over the surface of the electrolyte solution, to avoid unwanted turbulence and noise. Nitrite was added every 100 s with a micropipette from two solutions with a known nitrite concentration (0.05 M for 1–10 μM and 0.25 M for 20–100 μM), prepared adding NaNO_2

(ReagentPlus®, $\geq 99.0\%$, Sigma Aldrich) to PBS solution (final error on volumes $< 0.1\%$).

From the analysis, the potential (or the current density) variations were calculated as follows: (1) the first point was calculated as an average over 10 points before the step induced by nitrite addition. After the addition, (2) the system was left for 50 s to stabilize from transient effects and, in the following 50 s, a new point was extrapolated by 10-points-averaging 20 s before the step due to the next addition. The potential (vs RHE) (or the current density) variations were plotted vs the logarithm of the nitrite concentration and a linear fit was performed.

2.5. Catalytic layer stability, selectivity, and reversibility study

The stability of the catalytic layer was evaluated after the conditioning of the electrocatalyst and the first CV collected in oxygen-saturated electrolyte. The test consisted in a 12 h stability at OCP, spinning the electrode at 1600 rpm in O_2 -saturated electrolyte solution. The selectivity tests were performed by acquiring CVs and CPs, as previously described, in an O_2 -saturated PBS electrolyte solution containing further anions, such as chloride (Cl^-), nitrate (NO_3^-), and perchlorate (ClO_4^-). After 1000 s of stabilization, the three anions were added separately every 100 s in concentration of 10 μM each, followed by the addition of nitrite. The reversibility test was performed carrying out a sensing test (CP, 1–100 μM), followed by a stripping procedure in N_2 -purged 0.1 M PBS cycling the potential from 0.45 to 0.35 V vs RHE at a scan rate of 10 mV s^{-1} . After this step, the electrolyte solution was replaced after washing the glass cell with hot water and purged with oxygen for 20 min. A new CV was then collected to set the current density for acquiring CPs with a new addition of nitrite in the 1–100 μM range.

3. Results and discussion

3.1. Preliminary considerations on the role of the catalytic layer

The sensor in its constituents is represented by the catalytic layer deposited onto the glassy carbon of the rotating disk electrode (RDE), creating an interface with the electrolyte solution, containing both molecular oxygen and nitrite. The catalytic layer, composed by the electrocatalyst itself and an appropriate ionomer as binder, is then to be optimized to be exploited as nitrite sensor. A former study on nitrite poisoning of PGM-free electrocatalysts, adopted a catalytic layer composed of 0.17 mg cm^{-2} of electrocatalyst and 150 $\mu\text{L mL}^{-1}$ of Nafion 0.5 wt% for the 0.5–50 mM range [35]. Considering the nitrite concentration in wastewater is generally lower than 2.5 mg L^{-1} (ca. 55 μM) a new optimum in terms of ink formulation must be determined.

Three different catalyst loadings of 0.1, 0.135, and 0.17 mg cm^{-2} were chosen for the optimization study. Since the interaction of the electrocatalyst with the electrolyte solution is a matter of surface accessibility, a reduction in the loading would improve the surface dispersion, hence the material response to the presence of nitrite. However, a reduction in catalyst loading will also decrease the overall ORR activity. Thus, 0.1 mg cm^{-2} electrocatalyst loading can be considered the lower limit to obtain a satisfactory deposition, avoiding an incomplete coverage of the electrode surface. Increasing too much the electrocatalyst loading is not a proper choice either, for it leads to the increase of the thickness of the catalytic layer. Considering that reactions are occurring within the layer, intermediate species or external compounds can be trapped inside thicker layer or blocked before reaching the deepest active sites [38–41].

Regarding the Nafion content, the proton conducting polymer has the primary function of binder for the fine powder-like catalyst, to form the layer itself and to adhere to the electrode sur-

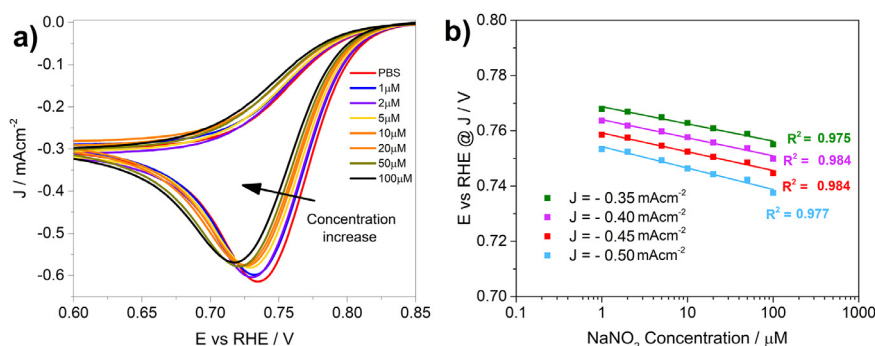


Fig. 1. Representative of the rational for the sensor; (a) CV of Fe-BZIM electrocatalyst at the increase of nitrite concentration (1–100 μM) for the case of 0.1 mg cm^{-2} –150 $\mu\text{L mL}^{-1}$. (b) Linear fit trends of potential vs nitrite concentration extrapolated from CVs at fixed current densities along the faradaic peak of oxygen reduction, and respective R^2 results. All the data concerning electrocatalyst loading variation and Nafion decrease are reported in Figs. S1 and S2.

face. However, if present at high content, Nafion can act as a capping agent of the catalytic layer, preventing direct access to the active sites, but leaving oxygen diffusion-through unaffected [35]. The volume of 150 μL of Nafion 0.5 wt% per mL of catalytic ink is a common value chosen for benchmark purpose and has been used extensively in the literature [26,35,42–45]. The lower value of 100 $\mu\text{L mL}^{-1}$ was evaluated for the catalyst loading optimization and cost reduction.

A further reduction in Nafion content is considered not viable because it could lead to issues in proton-conducting capability and delamination of the layer due to insufficient mechanical stability. This phenomenon is likely to occur in the hydrodynamic conditions used to eliminate the oxygen concentration gradient in the proximity of the surface. Table 1 summarizes the different electrocatalyst layers prepared.

Fig. 1a shows CV curves for a representative catalytic layer in O_2 -saturated PBS with increasing concentration of nitrite (in the range 1–100 μM). All the CVs resulting from the three different electrocatalyst loadings and Nafion content of 150 $\mu\text{L mL}^{-1}$ are reported in Fig. S1. The presence of the strong faradaic reduction peak around 0.75 V vs RHE is associated to the oxygen reduction processes catalyzed by the FeBZIM electrocatalyst. As the nitrite concentration increased, the reduction peak position shifted towards lower potential (higher overpotential) and peak current density decreased. This behavior is compatible with the site-blocking effect of nitrosyl ligand formed upon nitrite interaction with the $\text{Fe-N}_x\text{-C}$ coordination [34]. The effect of the interaction is then quantifiable extrapolating the potential (E) variations at fixed current densities, as shown in Fig. 1b. E linearly decreased with the logarithm of the nitrite concentration, resulting in a well-defined trend with R^2 values higher than 0.9 (Figs. 1b, and S1d–f). The correlation of ORR activity losses in the presence of nitrite molecules, along with good correlation coefficients, suggest PGM-free electrocatalyst can be used for nitrite sensing.

As expected, the modification of electrocatalyst loading and Nafion content modified the response of the system. Decreasing the catalyst loading led to a decrease in the faradaic peak intensity (Fig. S1a–c), indicating lower electrocatalytic activity. In addition, the averaged R^2 values (average \pm standard deviation) increased ranging from 0.961 ± 0.012 , 0.967 ± 0.003 , and 0.980 ± 0.005 , respectively for 0.17–150, 0.135–150, and 0.1–150. Among the three, the lowest standard deviation was achieved with the conditions 0.135–150, corresponding also to the highest sensitivity. The best R^2 value was achieved for the current density point of -0.45 mA cm^{-2} located in the peak area linked to the ORR in its full evolution.

The results of reduced Nafion content (100 $\mu\text{L mL}^{-1}$, Fig. S2a–f) on CVs are similar to those discussed above, with the peak area

reducing accordingly with the loading decrease. However, the extrapolated data at various current densities have linear trends with lower R^2 values. The averaged linear regression coefficients for the three loadings are 0.958 ± 0.011 (0.17–100), 0.943 ± 0.003 (0.135–100), and 0.935 ± 0.013 (0.1–100), respectively. Despite the lower R^2 compared to the 150 $\mu\text{L mL}^{-1}$, the sample with the lowest standard deviation is again the one with an electrocatalyst loading of 0.135 mg cm^{-2} . In this case, the highest slope is obtained for both 0.135–100 and 0.1–100, respectively at -0.45 mA cm^{-2} and -0.25 mA cm^{-2} .

The reason of the different trend in R^2 for the two Nafion content can be ascribed to differences in the oxygen management of the two layers. In the static condition of CV, the conversion of O_2 at the electrode surface creates a concentration gradient respect to the bulk of the solution, limiting the reaction. With the Nafion contained in the electrocatalytic layer, the consumption of O_2 inside the layer is affected by the diffusion through an additional polymer/electrocatalyst interface. If the Nafion is considered as a catalyst's buffer of oxygen molecules trapped within the layer, lowering the Nafion content led to a simplified intake of O_2 to the active sites and consequently in a more direct effect of O_2 decrease on the linear trends, resulting in more realistic R^2 values. As a result, the oxygen concentration during the evolving of the ORR, considered from the point of view of nitrite detection, should be kept constant to elide additional factors to the modification of the faradaic peaks. The expected solution for this peculiar issue relies in the nitrite sensing carried out at hydrodynamic condition.

3.3. Chronopotentiometry experiments for nitrite sensing

The hydrodynamic conditions were set at the rotation speed of 1600 rpm, a standard value used for ORR benchmarks. The electrode rotation is the ideal solution to avoid the local mass transfer limitations due to the O_2 concentration gradient in proximity of the electrode surface. In addition, the hydrodynamic condition helped to improve the sensitivity of the system stabilizing the noise and in parallel mixing the nitrite, avoiding further external interaction that could interfere with the measurement. Chronopotentiometry (CP) experiments were then carried out holding a specific current density at a constant value and measuring the variation of the potential of RDE over time when nitrite is added to the O_2 -saturated electrolyte solution.

Fig. S3 shows the protocol used for the selection of the current density values for the experiments, as the current density delivered by the system at the half-maximum of the faradaic peak of CVs. Any other values below this point are also a possible choice for the tests.

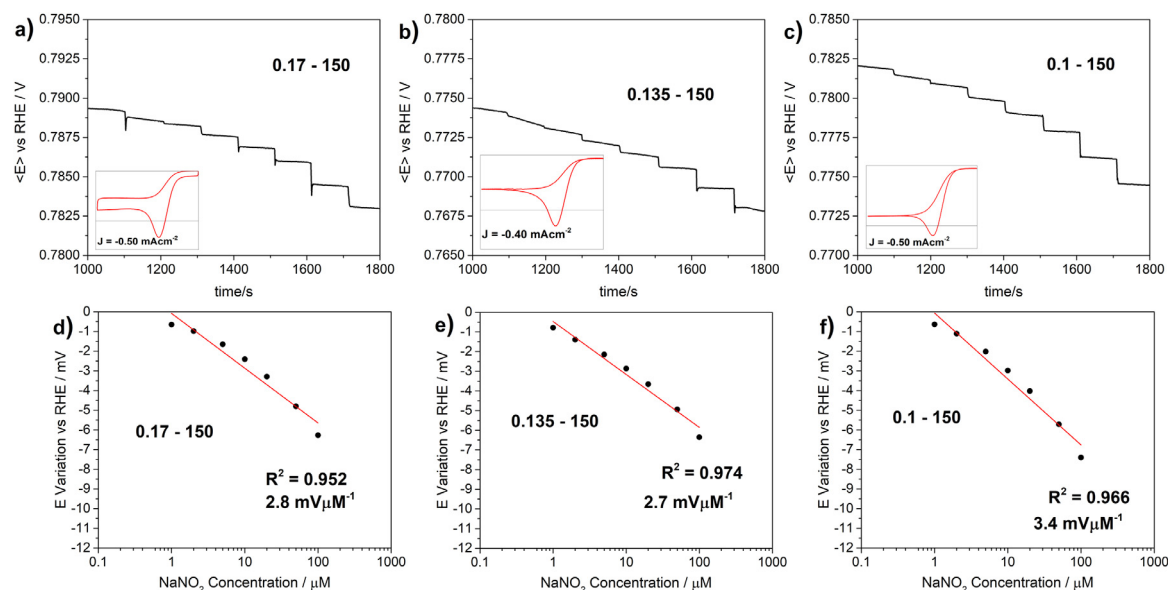


Fig. 2. Chronopotentiometry tests (averaged potential, in a 15 mV range) for nitrite sensing (0–100 μM range) with a Nafion content of 150 $\mu\text{L mL}^{-1}$ at the variation of electrocatalyst loading (a) 0.17–150, (b) 0.135–150, (c) 0.1–150. The Current density applied to collect the CP is reported in inset. Linear fit of potential decrease from the starting point (0 μM) of (d) 0.17–150, (e) 0.135–150, (f) 0.1–150.

The CP tests and the respective linear fit are reported in Fig. 2a–c and Fig. 2d–f, respectively. The current density applied to each test is indicated in the inset of each CP and depends on the specific deposition. Three electrocatalyst loadings were evaluated maintaining the Nafion content constant to 150 $\mu\text{L mL}^{-1}$. In the nitrite concentration range of 0–100 μM , the system underwent a constant and reproducible step variation upon nitrite addition. For the three catalyst loadings, CP experiments allowed improving the response in terms of linear regression coefficient of 0.135 mg cm^{-2} , as compared to cyclic voltammetry. The R^2 values obtained are 0.952, 0.974, and 0.966 with sensitivity of 2.8, 2.7, and 3.4 $\text{mV } \mu\text{M}^{-1}$, respectively for 0.17, 0.135, and 0.1 mg cm^{-2} (Fig. 2d–f).

As a complement of the study, the Limit of Detection (LOD) for each sample calculated using $3\sigma_N/S$, where σ_N is the standard deviation or noise of the signal and S is the signal value in mg L^{-1} , is reported in Fig. S4a. As shown, the LOD values with a Signal-to-noise (S/N) ratio above 3 lie in the range of nM with an absolute minimum for 0.135–150, a relative minimum for 0.1–150, and a maximum for 0.17–150. All the tests presented an underlying average drift of 2.25 $\mu\text{V s}^{-1}$ very likely associated to leakages of oxygen from the inside of the cell thorough one of the openings used to add the analyte.

Identical CP tests with the addition of nitrite in the concentration range of 0–100 μM , were also conducted using the catalytic ink prepared with 100 $\mu\text{L mL}^{-1}$ Nafion binder. The CPs are presented in Fig. 3a–c and the linear fits are presented in Fig. 3d–f with sensitivity of 2.8, 3.9, and 3.0 $\text{mV } \mu\text{M}^{-1}$, respectively for samples 0.17–100, 0.135–100, and 0.1–100. In this case, the hydrodynamic condition implementation resulted in improvements for all the R^2 values. Comparing these results with the ones reported in Fig. S2d–f for the half-maximum J (lowest J reported), is possible to quantify the increase. The 0.17–100 sample operated in hydrodynamic CP shown the lowest increase to a value of 0.957. This can be associated to a high-thickness layer not optimal for the μM range. The 0.1–100 improved to 0.966 while the 0.135–100 reached the maximum with the highest R^2 value of 0.995. The reported result of 0.135–100 is then comparable with the literature of nitrite sensors based on oxidation of nitrite on carbonaceous-modified electrodes as reported in Table 2 [19,20,46–52].

The LOD for Nafion 100 are reported in Fig. S4b. As can be seen comparing LOD results of Nafion 100 with Nafion 150, the decrease of ionomeric binder content affected the limit of detection of the system. For 0.17–100 the LOD is 30% lower than 0.17–150, for 0.135–100 is 55% lower than 0.135–150, while for 0.1–100 there is a 45% increase. All the test presented an underlying average drift of 3.02 $\mu\text{V s}^{-1}$ associated again to the equipment setup.

Based on CP tests, the catalytic layer with an electrocatalyst loading of 0.135 mg cm^{-2} and 100 $\mu\text{L mL}^{-1}$ of Nafion 0.5 wt.% is the optimum for the chosen concentration interval. To further improve the results, additional tests are conducted on the optimum, in the same concentration interval and compared to analogous tests run using the CA protocol (extrapolated potential instead of current density). The results, along with tolerance intervals, are reported in the supplementary information (Fig. S5). Considering mainstream potentiostats are designed mainly to operate on the management of low currents, the errors on the CA measurements are lower compared to the CPs. However, in the same range 1–100 μM the R^2 values performed weighting the data for their tolerances, are 0.964 for the averaged CA and 0.991 for the analogous averaged CP with sensitivity of 34.7 $\mu\text{A cm}^{-2} \mu\text{M}^{-1}$ and 3.4 $\text{mV } \mu\text{M}^{-1}$, respectively. Reducing the concentration interval helped to improve the correlation coefficients. In the range 1–50 μM , the R^2 increased to 0.968 (33.7 $\mu\text{A cm}^{-2} \mu\text{M}^{-1}$) and 0.996 (3.3 $\text{mV } \mu\text{M}^{-1}$), respectively for CA and CP. The further reduction to the 1–20 μM range additional improved the values, but again the CA protocol resulted in lower correlation coefficient, with just 0.974 (31.8 $\mu\text{A cm}^{-2} \mu\text{M}^{-1}$) compared to 0.998 (3.1 $\text{mV } \mu\text{M}^{-1}$) of the CP tests. For the averaged CP tests reported, the LOD value is found to be 0.53 μM ($S/N > 3$).

3.6. Catalytic layer stability, selectivity, and reversibility tests

After the selection of the appropriate electrocatalyst loading (0.135 mg cm^{-2}) and Nafion content within the ink preparation (100 $\mu\text{L mL}^{-1}$), stability, selectivity, and reversibility tests of the catalytic layer were carried out. Particularly, Fe-BZIM was subject to stability test (without the addition of nitrite) at OCP for 12 h as shown in Fig. 4a. The three tests run showed a good stability of

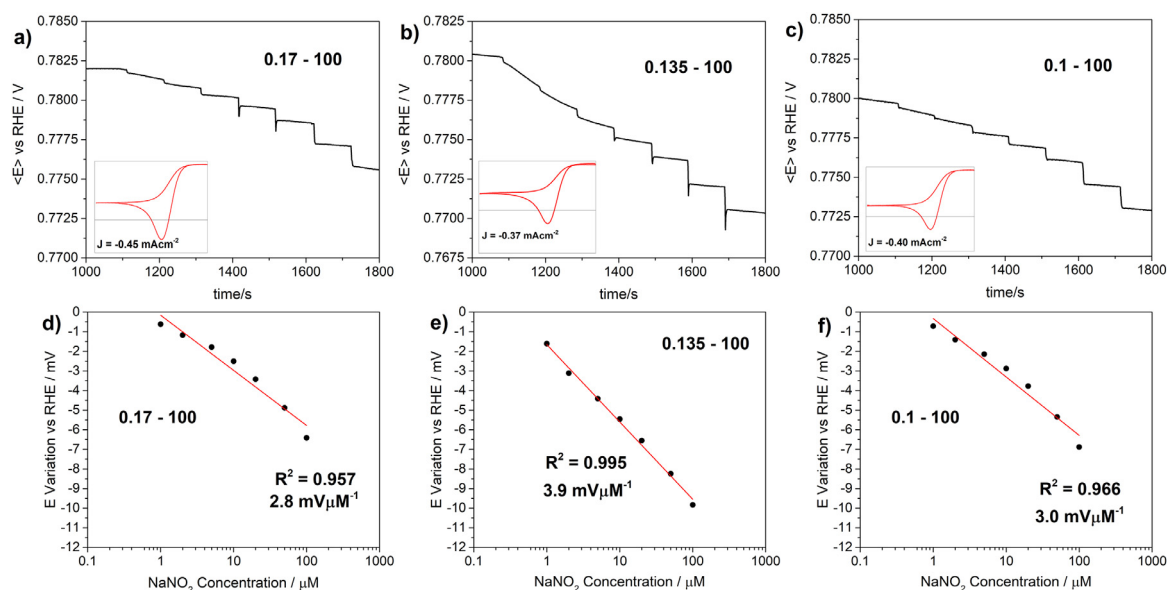


Fig. 3. Chronopotentiometry tests (averaged potential, in a 15 mV range) for nitrite sensing (0–100 μM range) with a Nafion content of 100 $\mu\text{L mL}^{-1}$ at the variation of electrocatalyst loading (a) 0.17–100, (b) 0.135–100, (c) 0.1–100. The current density applied to collect the CP is reported in inset. Linear fit of potential decrease from the starting point (0 μM) of (d) 0.17–100, (e) 0.135–100, (f) 0.1–100.

Table 2

Comparison with literature of sensing parameters for the new sensing methodology proposed.

Refs.	Type	technique	linearity	R^2	LOD
[46]	nitrite OX	amperometric	2–164 μM	0.998	1.44 μM
[47]	nitrite OX	amperometric	0.5 μM –2 mM	0.999	0.2 μM
[48]	nitrite OX	amperometric	20–800 μM	0.998	2.1 μM
[49]	nitrite OX	amperometric	1–380 μM	0.999	0.14 μM
[50]	nitrite OX	amperometric	1 μM –2 mM	0.999	0.0014 μM
[20]	nitrite OX	amperometric	0.3–720 μM	0.998	0.1 μM
[51]	nitrite OX	amperometric	0.1–3 mM	0.999	33 μM
[52]	nitrite OX	amperometric	0.5 μM –5 mM	0.998	0.2 μM
[19]	nitrite OX	amperometric	0.1–3838.5 μM	0.997	0.07 μM
This work	ORR	potentiometric	1–20 μM	0.998	0.53 μM

the deposited layer in the hydrodynamic conditions over the entire test. After a rapid decrease likely due to capacitive discharge effects, the OCP values stabilized at an average of 0.955 ± 0.005 V for the remaining of the test. PEIS analysis (data not shown) before and after the stability tests, reported no modification of the catalytic layer parameters due to the conditions of the protocol setup. The decrease in the Nafion content hence did not affect the stability properties of the layer.

Regarding the selectivity, the interaction of nitrite with PGM-free electrocatalysts is known to be specific toward the metal contained in the $\text{Fe-N}_x\text{-C}$ coordination. In addition, in the case of multiple contaminants the system is known to respond with a preferential interaction with nitrite [35], as reported in Fig. 4b for three different tests. The CP tests run in hydrodynamic conditions with O_2 -saturated PBS, showed no effect on the potential output of the system when up to 10 μM (each) of chloride, nitrate, and perchlorate were added one after the other every 100 s. After these, the addition of 10 μM of nitrite as a final analyte resulted in a clearly visible step of 1.87 ± 0.33 mV with no issues related to the presence of the other anions.

The problem concerning the reversibility of the $\text{Fe-N}_x\text{-C}$ /nitrite system was already assessed [35]. It was shown that the $\text{Fe-N}_x\text{-C}$ ORR electrocatalyst is prone to regeneration upon cycling the applied potentials at low negative values (from 0.45 to -0.35 V vs RHE) in N_2 -purged electrolyte [33,34]. This regeneration was found to be complete prevalently with high catalytic loading and

high Nafion content [35]. In this case, since the nitrite concentration is three orders of magnitude lower compared to our previous study, the complete saturation of the active sites was not reached. In this context, the uncomplete saturation of $\text{Fe-N}_x\text{-C}$ active sites was translated into the possibility to reuse a single deposition performing additional tests. In Fig. 4c, it is possible to notice that the stripping procedure did not reverse the contaminated condition of the deposited layer. Indeed, the second CV in the same conditions (5 mVs^{-1} , O_2 -saturated electrolyte) collected after the first sensing test in the 1–100 μM range and after the stripping procedure, reported a faradaic peak with a reduced area and shifted position. However, if the new CV is considered as evaluator for the current density to be applied to a new CP test, and the test was performed after replacing the electrolyte solution with new O_2 -purged solution, the system can withstand a second contamination with good results (Fig. 4d). This result can be ascribed to the incomplete saturation of the high number of active sites contained in the material.

3.7. Future directions and cost estimation

Based on the abovementioned results, further improvements can be applied using rotating working electrodes with smaller diameter. This could optimize the quality of depositions made with lower electrocatalyst content, thus lowering the nitrite LOD. Further, the sensor design can be modified to work with a static electrode immersed in a stirred solution, excluding the rotor and

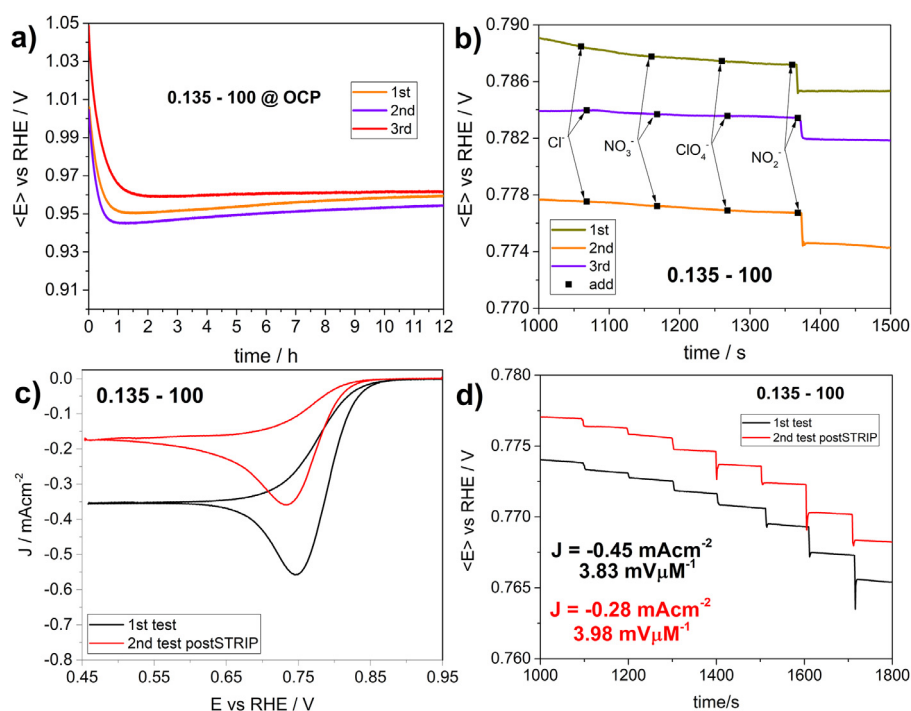


Fig. 4. (a) Additional results for 0.135–100 (a) Catalytic layer stability tests at Open Circuit Voltage (OCP) for 12 h at 1600 rpm. (b) Selectivity CP at 1600 rpm tests for 0.135–100 in the presence of three additional contaminants (10 μM each of Cl⁻, NO₃⁻, ClO₄⁻) each added consecutively every 100 s before the addition of 10 μM of nitrite. (c) CV collected before the 1st test and before the 2nd test but after the stripping procedure in N₂ was applied. (d) CP test in the range 1–100 μM with the proper current density applied obtained from the CV of (c). Current density values reported in inset.

RDE system, thus lowering the cost. In addition, implementation in terms of preparation time reduction can be obtained, skipping the conditioning and background recording in N₂, and operating directly in O₂ accounting for a fixed value normalization of the O₂-collected cyclic voltammetry.

An estimation of the material costs for the same Fe-N_x-C electrocatalyst family used in this experimentation was previously reported [40]. The material cost was estimated roughly in 3.5 USD g⁻¹ while the cost of Nafion is 6 USD ml⁻¹ (Sigma Aldrich). Considering a final electrocatalyst loading of 0.135 mg cm⁻², a 5 mm diameter electrode and 100 μL mL⁻¹ of 0.5 wt.% of Nafion as binder, with 1 USD would be possible to deposit nearly 2000 sensing layers. Nevertheless, considering the tests are performed using a standard rotor and rotating disk electrode instead of a standalone electrode, equipment costs must be taken in consideration.

4. Conclusions

The preliminary assessment of a new methodology for nitrite sensing using PGM-free electrocatalysts material is presented. The quantification of nitrite content is possible through the O₂ inhibition of Fe-N_x-C active sites upon interaction with NO₂⁻ molecules and the formation of the nitrosyl ligand. Using cyclic voltammetry and chronopotentiometry at 1600 rpm with the optimal current density set at the half-maximum of the faradaic peak, it was possible to select the best conditions for nitrite sensing in the 1–100 μM range. This corresponded to an electrocatalyst loading of 0.135 mg cm⁻² and 100 μL mL⁻¹ Nafion content deposited over a 5 mm diameter electrode, which led to a LOD in the sub-μM range with a signal-to-noise (S/N) ratio > 3. The stability, selectivity and reversibility of the Fe-N_x-C/nitrite system was also evaluated. The catalytic layer was stable over a 12 h test at the OCP, the nitrite sensing was not affected by the presence of different contaminants like chloride, nitrate, and perchlorate added consecutively. In addition, due to the very low concentration of nitrite, the catalytic

layer sensor can be reused for additional tests since the active sites were not saturated. The cost per catalyst deposition was estimated around 0.00051 USD, with the possibility to perform at least two tests per deposition, which show promise for low-cost nitrite sensing applications.

Declaration of Competing Interest

The authors declare that they have no known competing financial interests or personal relationships that could have appeared to influence the work reported in this paper.

Acknowledgment

Carlo Santoro would like to acknowledge the support from the Italian Ministry of Education, Universities and Research (Ministero dell'Istruzione, dell'Università e della Ricerca – MIUR) through the “Rita Levi Montalcini 2018” Fellowship (Grant number PGR18MAZLI). Carlo Santoro would like to acknowledge the support from the Italian Ministry of University and Research (MIUR) through grant “Dipartimenti di Eccellenza – 2017 – Materials for energy”. Enrico Marsili was financially supported by Collaborative Research Program 021220CRP0522, Nazarbayev University, Kazakhstan.

Supplementary materials

Supplementary material associated with this article can be found, in the online version, at doi:10.1016/j.electacta.2021.139514.

References

- [1] O. US EPA National Primary Drinking Water Regulations, US EPA, 2015 <https://www.epa.gov/ground-water-and-drinking-water/national-primary-drinking-water-regulations>.

- [2] EU Council, Council directive 98/83/EC on the quality of water intended for human consumption, (2015). <https://eur-lex.europa.eu/legal-content/EN/TXT/?uri=CELEX%3A01998L0083-20151027>.
- [3] G.M. Greenway, S.J. Haswell, P.H. Petsul, Characterisation of a micro-total analytical system for the determination of nitrite with spectrophotometric detection, *Anal. Chim. Acta* 387 (1999) 1–10, doi:10.1016/S0003-2670(99)00047-1.
- [4] H. Kodamatani, S. Yamazaki, K. Saito, T. Tomiyasu, Y. Komatsu, Selective determination method for measurement of nitrite and nitrate in water samples using high-performance liquid chromatography with post-column photochemical reaction and chemiluminescence detection, *J. Chromatogr. A* 1216 (2009) 3163–3167, doi:10.1016/j.chroma.2009.01.096.
- [5] B.R. Kozub, N.V. Rees, R.G. Compton, Electrochemical determination of nitrite at a bare glassy carbon electrode; why chemically modify electrodes? *Sens. Actuators B Chem.* 143 (2010) 539–546, doi:10.1016/j.snb.2009.09.065.
- [6] Z. Yilong, Z. Dean, L. Daojiang, Electrochemical and other methods for detection and determination of dissolved nitrite: a review, *Int. J. Electrochem. Sci.* 10 (2015) 25.
- [7] L. He, K. Zhang, C. Wang, X. Luo, S. Zhang, Effective indirect enrichment and determination of nitrite ion in water and biological samples using ionic liquid-dispersive liquid-liquid microextraction combined with high-performance liquid chromatography, *J. Chromatogr. A* 1218 (2011) 3595–3600, doi:10.1016/j.chroma.2011.04.014.
- [8] P. Singh, M.K. Singh, Y.R. Beg, G.R. Nishad, A review on spectroscopic methods for determination of nitrite and nitrate in environmental samples, *Talanta* 191 (2019) 364–381, doi:10.1016/j.talanta.2018.08.028.
- [9] X. Yin, Q. Chen, H. Song, M. Yang, H. Wang, Sensitive and selective electrochemiluminescent detection of nitrite using dual-stabilizer-capped CdTe quantum dots, *Electrochem. Commun.* 34 (2013) 81–85, doi:10.1016/j.elecom.2013.04.029.
- [10] X. Liu, L. Guo, L. Cheng, H. Ju, Determination of nitrite based on its quenching effect on anodic electrochemiluminescence of CdSe quantum dots, *Talanta* 78 (2009) 691–694, doi:10.1016/j.talanta.2008.12.035.
- [11] Q.H. Wang, L.J. Yu, Y. Liu, L. Lin, R. Lu, J. Zhu, L. He, Z.L. Lu, Methods for the detection and determination of nitrite and nitrate: a review, *Talanta* 165 (2017) 709–720, doi:10.1016/j.talanta.2016.12.044.
- [12] M.A.P. Mahmud, F. Ejeian, S. Azadi, M. Myers, B. Pejic, R. Abbassi, A. Razmjou, M. Asadnia, Recent progress in sensing nitrate, nitrite, phosphate, and ammonium in aquatic environment, *Chemosphere* 259 (2020) 127492, doi:10.1016/j.chemosphere.2020.127492.
- [13] V. Rosca, M. Duca, M.T. De Groot, M.T.M. Koper, Nitrogen cycle electrocatalysis, *Chem. Rev.* 109 (2009) 2209–2244, doi:10.1021/cr8003696.
- [14] B. Piela, P.K. Wrona, Oxidation of nitrites on solid electrodes: I. Determination of the reaction mechanism on the pure electrode surface, *J. Electrochem. Soc.* 149 (2002) E55, doi:10.1149/1.1433751.
- [15] B. Piela, P. Piela, P.K. Wrona, Oxidation of nitrite on solid electrodes: II. Determination of the reaction mechanism on surfaces covered by an oxide layer, *J. Electrochem. Soc.* 149 (2002) E357, doi:10.1149/1.1502691.
- [16] X. Xing, D.A. Scherson, Electrochemical oxidation of nitrite on a rotating gold disk electrode: a second-order homogeneous disproportionation process, *Anal. Chem.* 60 (1988) 1468–1472, doi:10.1021/ac00165a023.
- [17] G. Li, Y. Xia, Y. Tian, Y. Wu, J. Liu, Q. He, D. Chen, Review-recent developments on graphene-based electrochemical sensors toward nitrite, *J. Electrochem. Soc.* 166 (2019) B881–B895, doi:10.1149/2.0171912jes.
- [18] D. Li, T. Wang, Z. Li, X. Xu, C. Wang, Y. Duan, Application of graphene-based materials for detection of nitrate and nitrite in water—a review, *Sensors* 20 (2019) (Basel), doi:10.3390/s20010054.
- [19] W. Zhu, Y. Zhang, J. Gong, Y. Ma, J. Sun, T. Li, J. Wang, Surface engineering of carbon fiber paper toward exceptionally high-performance and stable electrochemical nitrite sensing, *ACS Sens.* 4 (2019) 2980–2987, doi:10.1021/acssensors.9b01474.
- [20] P. Wang, M. Wang, F. Zhou, G. Yang, L. Qu, X. Miao, Development of a paper-based, inexpensive, and disposable electrochemical sensing platform for nitrite detection, *Electrochem. Commun.* 81 (2017) 74–78, doi:10.1016/j.elecom.2017.06.006.
- [21] N. Pankratova, M. Cuartero, T. Cherubini, G.A. Crespo, E. Bakker, In-line acidification for potentiometric sensing of nitrite in natural waters, *Anal. Chem.* 89 (2017) 571–575, doi:10.1021/acs.analchem.6b03946.
- [22] M. Cuartero, G.A. Crespo, All-solid-state potentiometric sensors: a new wave for *in situ* aquatic research, *Curr. Opin. Electrochem.* 10 (2018) 98–106, doi:10.1016/j.coelec.2018.04.004.
- [23] T. Asset, P. Atanassov, Iron-nitrogen-carbon catalysts for proton exchange membrane fuel cells, *Joule* 4 (2020) 33–44, doi:10.1016/j.joule.2019.12.002.
- [24] A. Zitolo, V. Goellner, V. Armel, M.T. Sougrati, L. Mineva, L. Stievano, E. Fonda, F. Jaouen, Identification of catalytic sites for oxygen reduction in iron- and nitrogen-doped graphene materials, *Nat. Mater.* 14 (2015) 937–942, doi:10.1038/nmat4367.
- [25] K. Artyushkova, A. Serov, S. Rojas-Carbonell, P. Atanassov, Chemistry of multitudinous active sites for oxygen reduction reaction in transition metal-nitrogen-carbon electrocatalysts, *J. Phys. Chem. C* 119 (2015) 25917–25928, doi:10.1021/acs.jpcc.5b07653.
- [26] S. Rojas-Carbonell, K. Artyushkova, A. Serov, C. Santoro, I. Matanovic, P. Atanassov, Effect of pH on the activity of platinum group metal-free catalysts in oxygen reduction reaction, *ACS Catal.* 8 (2018) 3041–3053, doi:10.1021/acscatal.7b03991.
- [27] J. Li, F. Jaouen, Structure and activity of metal-centered coordination sites in pyrolyzed metal-nitrogen-carbon catalysts for the electrochemical reduction of O₂, *Curr. Opin. Electrochem.* 9 (2018) 198–206, doi:10.1016/j.coelec.2018.03.039.
- [28] B. Mecheri, V.C.A. Ficca, M.A. Costa de Oliveira, A. D'Epifanio, E. Placidi, F. Arciprete, S. Licoccia, Facile synthesis of graphene-phthalocyanine composites as oxygen reduction electrocatalysts in microbial fuel cells, *Appl. Catal. B Environ.* 237 (2018) 699–707, doi:10.1016/j.apcatb.2018.06.031.
- [29] M.A. Costa De Oliveira, A. D'Epifanio, H. Ohnuki, B. Mecheri, Platinum group metal-free catalysts for oxygen reduction reaction: applications in microbial fuel cells, *Catalysts* 10 (2020) 475, doi:10.3390/catal10050475.
- [30] W. Da, S. Freitas, A. D'Epifanio, V.C.A. Ficca, E. Placidi, F. Arciprete, B. Mecheri, Tailoring active sites of iron-nitrogen-carbon catalysts for oxygen reduction in alkaline environment: effect of nitrogen-based organic precursor and pyrolysis atmosphere, *Electrochim. Acta* 391 (2021) 138899, doi:10.1016/j.electacta.2021.138899.
- [31] A. Kozhushner, N. Zion, L. Elbaz, Methods for assessment and measurement of the active site density in platinum group metal-free oxygen reduction reaction catalysts, *Curr. Opin. Electrochem.* (2020) 100620, doi:10.1016/j.coelec.2020.08.002.
- [32] C. Santoro, A. Serov, K. Artyushkova, P. Atanassov, Platinum group metal-free oxygen reduction electrocatalysts used in neutral electrolytes for bioelectrochemical reactor applications, *Curr. Opin. Electrochem.* 23 (2020) 106–113, doi:10.1016/j.coelec.2020.06.003.
- [33] D. Malko, A. Kucernak, T. Lopes, *In situ* electrochemical quantification of active sites in Fe–N/C non-precious metal catalysts, *Nat. Commun.* 7 (2016) 13285, doi:10.1038/ncomms13285.
- [34] D. Malko, A. Kucernak, T. Lopes, Performance of Fe–N/C oxygen reduction electrocatalysts toward NO₂[−], NO, and NH₂OH electroreduction: from fundamental insights into the active center to a new method for environmental nitrite destruction, *J. Am. Chem. Soc.* 138 (2016) 16056–16068, doi:10.1021/jacs.6b09622.
- [35] V.C.A. Ficca, C. Santoro, A. D'Epifanio, S. Licoccia, A. Serov, P. Atanassov, B. Mecheri, Effect of active site poisoning on iron–nitrogen–carbon platinum-group-metal-free oxygen reduction reaction catalysts operating in neutral media: a rotating disk electrode study, *ChemElectroChem* 7 (2020) 3044–3055, doi:10.1002/celec.202000754.
- [36] B. Mecheri, R. Gokhale, C. Santoro, M.A. Costa de Oliveira, A. D'Epifanio, S. Licoccia, A. Serov, K. Artyushkova, P. Atanassov, Oxygen reduction reaction electrocatalysts derived from iron salt and benzimidazole and aminobenzimidazole precursors and their application in microbial fuel cell cathodes, *ACS Appl. Energy Mater.* 1 (2018) 5755–5765, doi:10.1021/acsaem.8b01360.
- [37] D. Sebastián, A. Serov, K. Artyushkova, P. Atanassov, A.S. Aricó, V. Baglio, Performance, methanol tolerance and stability of Fe-aminobenzimidazole derived catalyst for direct methanol fuel cells, *J. Power Sources* 319 (2016) 235–246, doi:10.1016/j.jpowsour.2016.04.067.
- [38] S. Khandavalli, R. Iyer, J.H. Park, D.J. Myers, K.C. Neyerlin, M. Ulsh, S.A. Mauger, Effect of dispersion medium composition and ionomer concentration on the microstructure and rheology of Fe–N–C platinum group metal-free catalyst inks for polymer electrolyte membrane fuel cells, *Langmuir* 36 (2020) 12247–12260, doi:10.1021/acs.langmuir.0c02015.
- [39] L. Osmieri, G. Wang, F.C. Cetinbas, S. Khandavalli, J. Park, S. Medina, S.A. Mauger, M. Ulsh, S. Pylypenko, D.J. Myers, K.C. Neyerlin, Utilizing ink composition to tune bulk-electrode gas transport, performance, and operational robustness for a Fe–N–C catalyst in polymer electrolyte fuel cell, *Nano Energy* 75 (2020) 104943, doi:10.1016/j.nanoen.2020.104943.
- [40] C. Santoro, M. Kodali, S. Herrera, A. Serov, I. Ieropoulos, P. Atanassov, Power generation in microbial fuel cells using platinum group metal-free cathode catalyst: effect of the catalyst loading on performance and costs, *J. Power Sources* 378 (2018) 169–175, doi:10.1016/j.jpowsour.2017.12.017.
- [41] A. Bonakdarpour, M. Lefevre, R. Yang, F. Jaouen, T. Dahn, J.P. Dodelet, J.R. Dahn, Impact of loading in RRDE experiments on Fe–N–C catalysts: two- or four-electron oxygen reduction? *Electrochem. Solid State Lett.* 11 (2008) B105, doi:10.1149/1.2904768.
- [42] M. Kodali, C. Santoro, S. Herrera, A. Serov, P. Atanassov, Bimetallic platinum group metal-free catalysts for high power generating microbial fuel cells, *J. Power Sources* 366 (2017) 18–26, doi:10.1016/j.jpowsour.2017.08.110.
- [43] M.J. Workman, M. Dzara, C. Ngo, S. Pylypenko, A. Serov, S. McKinney, J. Gordon, P. Atanassov, K. Artyushkova, Platinum group metal-free electrocatalysts: effects of synthesis on structure and performance in proton-exchange membrane fuel cell cathodes, *J. Power Sources* 348 (2017) 30–39, doi:10.1016/j.jpowsour.2017.02.067.
- [44] R. Gokhale, Y. Chen, A. Serov, K. Artyushkova, P. Atanassov, Direct synthesis of platinum group metal-free Fe–N–C catalyst for oxygen reduction reaction in alkaline media, *Electrochem. Commun.* 72 (2016) 140–143, doi:10.1016/j.elecom.2016.09.013.
- [45] C. Santoro, S. Rojas-Carbonell, R. Awais, R. Gokhale, M. Kodali, A. Serov, K. Artyushkova, P. Atanassov, Influence of platinum group metal-free catalyst synthesis on microbial fuel cell performance, *J. Power Sources* 375 (2018) 11–20, doi:10.1016/j.jpowsour.2017.11.039.
- [46] H. Wu, S. Fan, X. Jin, H. Zhang, H. Chen, Z. Dai, X. Zou, Construction of a zinc porphyrin–fullerene-derivative based nonenzymatic electrochemical sensor for sensitive sensing of hydrogen peroxide and nitrite, *Anal. Chem.* 86 (2014) 6285–6290, doi:10.1021/ac500245k.
- [47] F. Xu, M. Deng, Y. Liu, X. Ling, X. Deng, L. Wang, Facile preparation of poly (di-allyldimethylammonium chloride) modified reduced graphene oxide for sensitive detection of nitrite, *Electrochem. Commun.* 47 (2014) 33–36, doi:10.1016/j.elecom.2014.07.016.

- [48] C.W. Kung, T.H. Chang, L.Y. Chou, J.T. Hupp, O.K. Farha, K.C. Ho, Porphyrin-based metal-organic framework thin films for electrochemical nitrite detection, *Electrochem. Commun.* 58 (2015) 51–56, doi:[10.1016/j.elecom.2015.06.003](https://doi.org/10.1016/j.elecom.2015.06.003).
- [49] Y. Haldorai, J.Y. Kim, A.T.E. Vilian, N.S. Heo, Y.S. Huh, Y.K. Han, An enzyme-free electrochemical sensor based on reduced graphene oxide/Co₃O₄ nanospindle composite for sensitive detection of nitrite, *Sens. Actuators B Chem.* 227 (2016) 92–99, doi:[10.1016/j.snb.2015.12.032](https://doi.org/10.1016/j.snb.2015.12.032).
- [50] Y. Haldorai, S.K. Hwang, A.I. Gopalan, Y.S. Huh, Y.K. Han, W. Voit, G. Sai-Anand, K.P. Lee, Direct electrochemistry of cytochrome c immobilized on titanium nitride/multi-walled carbon nanotube composite for amperometric nitrite biosensor, *Biosens. Bioelectron.* 79 (2016) 543–552, doi:[10.1016/j.bios.2015.12.054](https://doi.org/10.1016/j.bios.2015.12.054).
- [51] A.R. Marlinda, A. Pandikumar, N. Yusoff, N.M. Huang, H.N. Lim, Electrochemical sensing of nitrite using a glassy carbon electrode modified with reduced functionalized graphene oxide decorated with flower-like zinc oxide, *Microchim. Acta* 182 (2015) 1113–1122, doi:[10.1007/s00604-014-1436-x](https://doi.org/10.1007/s00604-014-1436-x).
- [52] D. Chen, J. Jiang, X. Du, Electrocatalytic oxidation of nitrite using metal-free nitrogen-doped reduced graphene oxide nanosheets for sensitive detection, *Talanta* 155 (2016) 329–335, doi:[10.1016/j.talanta.2016.05.003](https://doi.org/10.1016/j.talanta.2016.05.003).